ELSEVIER

International Journal of Pharmaceutics 107 (1994) 9–21

international journal of pharmaceutics

Development of a physical model for simultaneous diffusion/bioconversion of methotrexate dialkyl esters: A potential parallel/sequential metabolic scheme

James J. Fort [1], Ashim K. Mitra *

Department of Industrial and Physical Pharmacy, School of Pharmacy and Pharmacal Sciences, Purdue University, West Lafayette, IN 47907, USA

(Received 25 July 1989; Modified version received 23 August 1993; Accepted 30 November 1993)

Abstract

A physical model has been developed which accommodates simultaneous diffusion/parallel-sequential bioconversion process through hairless mouse skin. The model includes both tape-stripped and full-thickness skin to describe the diffusion/bioconversion of methotrexate (MTX) dialkyl esters, in which a potential parallel/sequential esterase metabolic scheme is operative. Simulations are also included to illustrate the behavior of MTX dialkyl esters with the simultaneous diffusion/bioconversion parameters in which the metabolism stops at the level of MTX monoalkyl esters.

Key words: Simultaneous diffusion/bioconversion; Parallel/sequential metabolic scheme; Concentration/distance profile; Hairless mouse skin simulation; Tape-stripped skin; Full-thickness skin; Methotrexate dialkyl ester

1. Introduction

The skin has been described in great detail with respect to its physical and biochemical characteristics (Bisser, 1987). Another manner in which the skin property can be described is in terms of the ability of drug molecules to diffuse through its layers. The aim of a mathematical treatment is to describe the diffusion process through the skin, taking into consideration the physical and chemical properties of the drug molecule and the properties of the membrane. Such an approach for a compound which is not only diffusing, but also undergoing biotransformation, can be very valuable in drug design illustrating the relative concentrations of the drug and its metabolites in the various skin layers. For instance, with existing knowledge of the physical properties of a limited number of derivatives, such as a few homologues in a series, it might be possible to design new molecules with optimum permeation and bioconversion parameters.

* Corresponding author.

The computer programs used for data simulation are available upon request from the authors.

[1] Present address: Abbott Laboratories, Pharmaceutical Products Division, North Chicago, IL 60064, U.S.A.

SSDI 0378-5173(93)E0366-X

A simplified version of the problem of simultaneous transport and bioconversion was discussed by Loftsson (1982) with the permeation of aspirin. The skin as a whole is represented metabolically by a single first order rate constant. Provision is also made for metabolism in the receptor phase. The final equation describing the process is a monoexponential expression.

A pharmacokinetic model, which treats the skin, donor and receptor phases as compartments has been described by Wallace and Barnett (1978). This model offers the flexibility of treating the skin as one or several compartments, e.g., each layer of the skin can be a compartment. Additionally, the model incorporates the parallel (paracellular) transport mechanism, whereby drug diffuses through various skin appendages (sweat glands, hair follicles, etc.). The model as described does not show a metabolic component to the skin, although this could be easily accounted for.

The most significant prodrug simultaneous transport/bioconversion model development was described in the literature in several articles. The beginning of this development describes a system, which depicts the skin as a two ply laminate, namely the stratum corneum and the cutaneous tissue (viable epidermis and dermis) (Ando et al., 1977a,b; Yu et al., 1979a). The compound utilized in the model is vidarabine 5′-valerate which is a prodrug first hydrolyzed to vidarabine, and subsequently deaminated, both of these reactions being enzymatic. This sequential metabolic pathway and the Fickian diffusion through the simplified skin membrane are incorporated into the model. Explicit final equations were developed describing the concentration vs distance profile for each of the three compounds. Assumptions in the model such as first order metabolism, sink conditions, as well as invariant diffusion coefficients in each layer with distance were utilized.

This model was also extended to accommodate the tape stripped model, in which the stratum corneum has been removed (Yu et al., 1979b). This altered membrane was used for parameter determinations, such as enzymatic rate constants and diffusion coefficients. It was found that the experimental data did not give an optimum fit to the bilaminate model, requiring a new model with increased complexity.

This newer physical model utilizing the same metabolic sequence previously described for vidarabine 5′-valerate was developed (Yu et al., 1980a). The skin has been described both metabolically and by its diffusion properties as a three-ply laminate consisting of the stratum corneum, viable epidermis, and dermis. Each layer has been assigned diffusion coefficients and metabolic rate constants with respect to each chemical species present in that layer. This treatment reflects the lack of homogeneity of enzymatic activity within the viable epidermis and dermis (Yu et al., 1980b). The viable epidermis is given more metabolic activity than the dermis, although this may not be totally accurate, as discussed later in this report. From a diffusion standpoint, the viable epidermis in the hairless mouse represents roughly a 10 μm thick layer, as compared to a 300–400 μm dermis. It is considerably more lipophilic and amounts to more of a diffusive barrier to a polar compound than the dermis (Yu et al., 1980c). Mathematically, this model is considerably more complicated, although the model assumptions are similar to the bilaminate case with respect to sink conditions and uniformity of enzyme activity and diffusivity within a particular layer. When experimental data were fitted by this model, there was better correlation than with the bilaminate case.

A later development was the construction of a physical model which was more general than the previous bi- and trilaminates (Fox et al., 1979). In this case the model did not limit itself to first order metabolism of prodrug or drug molecules. Provision was made for a saturable or Michaelis-Menten metabolic reaction. The general model also included the flexibility of adding an inhibitive component to the model. An example of this would be where the prodrug could inhibit the subsequent metabolism of the active drug or vice versa. As would be expected, the mathematics are even more complicated, entering into the realm of numerical solutions for the equations, e.g., no explicit solutions for concentration/distance expressions could be obtained.

This type of model was utilized to some extent

in a more recent study by the same group in which several vidarabine esters were evaluated for diffusive and metabolic characteristics within hairless mouse skin (Higuchi et al., 1983).

The purpose of this report is to develop a model similar in principles to those previously discussed when the potential metabolic scheme in skin is a combination of parallel and sequential steps.

The physical models described in this report will treat the full-thickness skin as a multilaminate utilizing principles similar to that proposed by Yu et al. (1980a). The most elegant and important feature of this model is that the trilaminate, consisting of a stratum corneum, viable epidermis, and dermis, not only is the most appropriate model, but also has the flexibility to collapse to a bilaminate (stratum corneum and cutaneous layer) in terms of either diffusivity or metabolic activity. In the latter model, the cutaneous layer is a composite of the viable epidermis and dermis. It is important to mention that models representing tape-stripped skin will also be derived. In this case, the trilaminate will lose one of its layers, e.g., the stratum corneum. This model will be referred to as the trilaminate stripped model.

The following mathematical development will use the general multilaminate approach which can be utilized for any number of layers. By employing the proper post-integration boundary conditions, the full-thickness and stripped models for both the bilaminate and trilaminate variants can be derived. These models are self-consistent in that when the parameters of the trilaminate's epidermis and dermis are the same, the model collapses to a bilaminate. For most compounds, the stratum corneum is the major rate-limiting barrier for dermal drug absorption and there may be little significant resistance boundary and enzymatic activity difference between the epidermis and dermis. Under this circumstance, the mathematical treatment will be greatly simplifies by collapsing the trilaminate model to a bilaminate one.

The derivation of the general multilaminate membrane model begins with the multilaminate shown schematically in Fig. 1. Each layer is considered to have the metabolic scheme shown in Fig. 2. The quantities, $k_{1,i}$–$k_{5,i}$ represent the first order metabolic rate constants in the i-th layer. The letters A–D represent diester, α-monester, γ-monester, and MTX, respectively. With such an approach, any number of layers can be modeled.

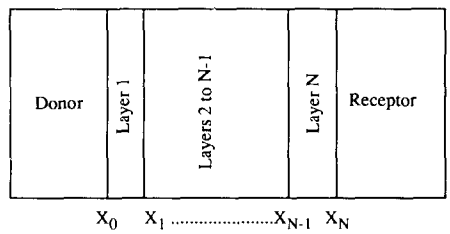

Fig. 1. Schematic diagram of skin depicted as a multilaminate membrane sandwiched between donor and receptor solutions.

For each layer, the following differential equations, representing the relationship between concentration and distance, can be written:

$$D_{A,i}\, d^2A/dx^2 - (k_{1,i} + k_{2,i} + k_{5,i})A = 0 \quad (1)$$

$$D_{B,i}\, d^2B/dx^2 - k_{3,i}B + k_{1,i}A = 0 \quad (2)$$

$$D_{C,i}\, d^2C/dx^2 - k_{4,i}C + k_{2,i}A = 0 \quad (3)$$

$$D_{D,i}\, d^2D/dx^2 + k_{3,i}B + k_{4,i}C + k_{5,i}A = 0 \quad (4)$$

Some other quantities will need to be defined:

$$a_i = \sqrt{[(k_{1,i} + k_{2,i} + k_{5,i})/D_{A,i}]} \quad (5)$$

$$b_i = \sqrt{(k_{3,i}/D_{B,i})} \quad (6)$$

$$c_i = \sqrt{(k_{4,i}/D_{C,i})} \quad (7)$$

$$U_A(x) = A/K_{A,i} \quad (8)$$

$$U_B(x) = B/K_{B,i} \quad (9)$$

$$U_C(x) = C/K_{C,i} \quad (10)$$

$$U_D(x) = D/K_{D,i} \quad (11)$$

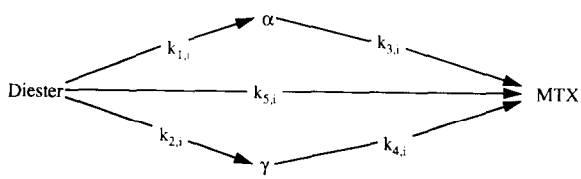

Fig. 2. Theoretical scheme for the parallel/sequential enzymatic hydrolysis of a MTX dialkyl ester in an individual layer of hairless mouse skin.

where $K_{A,i}$ to $K_{D,i}$ are the partition coefficients of each species in the i-th layer.

$$P_{A,i} = K_{A,i} D_{A,i} \quad (12)$$

$$P_{B,i} = K_{B,i} D_{B,i} \quad (13)$$

$$P_{C,i} = K_{C,i} D_{C,i} \quad (14)$$

$$P_{D,i} = K_{D,i} D_{D,i} \quad (15)$$

where $P_{A,i}$ to $P_{D,i}$ are the permeability coefficients of each species in the i-th layer.

The fluxes for each species in the i-th layer are as follows:

$$F_A(x) = -D_{A,i}\, dA/dx \quad (16)$$

$$F_B(x) = -D_{B,i}\, dB/dx \quad (17)$$

$$F_C(x) = -D_{C,i}\, dC/dx \quad (18)$$

$$F_D(x) = -D_{D,i}\, dD/dx \quad (19)$$

Several assumptions are inherent to these models. (1) The enzymes, non-specific esterases, are homogeneously distributed in each layer, except for the stratum corneum. (2) The stratum corneum is essentially permeable to the highly lipophilic diester prodrug and serves as a barrier preventing the back diffusion of the more hydrophilic α- and γ-monoesters and parent MTX. (3) The enzymatic reactions in the metabolically active tissues are parallel and sequential in nature and are irreversible. As previously mentioned, the rate constants for enzymatic hydrolysis are first order. (4) Diffusivities of all species in each layer are independent of distance. (5) Sink and steady-state conditions prevail. Most of the assumptions are based on known facts while some are supported by our own experimental data (Fort and Mitra, 1994; Fort et al., 1993, 1994). Although the second assumption, by eliminating the contribution of back diffusion, may not hold true for long-duration diffusion studies, it will greatly simplify the mathematical treatment.

The method of obtaining the general solutions for each of the concentration-distance differential equations is the same as with any homogeneous second order differential equation in the case of U_A. For U_B and U_C the method of undetermined coefficients has been employed. U_D is solved by inserting in the solutions for U_A, U_B, and U_C and integrating twice. The boundary conditions for all four differential equations are as follows:

$$U_A(x = 0) = U_A(x_{i-1}) \quad (20)$$

$$F_A(x_{i-1}) = P_{A,i}\, dU_A(x)/dx_{x=0} \quad (21)$$

where x_{i-1} is the boundary or interface between the previous layer and the layer in question.

Utilizing the above boundary conditions and the methods for obtaining general solutions, the final expressions for each species can be expressed conveniently in a matrix form.

$$\begin{bmatrix} U_{A,i}(x) \\ F_{A,i}(x) \\ U_{B,i}(x) \\ F_{B,i}(x) \\ U_{C,i}(x) \\ F_{C,i}(x) \\ U_{D,i}(x) \\ F_{D,i}(x) \end{bmatrix} = \begin{bmatrix} m_{i11} & m_{i12} & 0 & 0 & 0 & 0 & 0 & 0 \\ m_{i21} & m_{i22} & 0 & 0 & 0 & 0 & 0 & 0 \\ m_{i31} & m_{i32} & m_{i33} & m_{i34} & 0 & 0 & 0 & 0 \\ m_{i41} & m_{i42} & m_{i43} & m_{i44} & 0 & 0 & 0 & 0 \\ m_{i51} & m_{i52} & 0 & 0 & m_{i55} & m_{i56} & 0 & 0 \\ m_{i61} & m_{i62} & 0 & 0 & m_{i65} & m_{i66} & 0 & 0 \\ m_{i71} & m_{i72} & m_{i73} & m_{i74} & m_{i75} & m_{i76} & 1 & m_{i78} \\ m_{i81} & m_{i82} & m_{i83} & m_{i84} & m_{i85} & m_{i86} & 0 & 1 \end{bmatrix} \times \begin{bmatrix} U_A(x_{i-1}) \\ F_A(x_{i-1}) \\ U_B(x_{i-1}) \\ F_B(x_{i-1}) \\ U_C(x_{i-1}) \\ F_C(x_{i-1}) \\ U_D(x_{i-1}) \\ F_D(x_{i-1}) \end{bmatrix} \quad (22)$$

where:

$$m_{i11} = \cosh\, a_i x$$

$$m_{i12} = -\frac{\sinh\, a_i x}{P_{A,i} a_i}$$

$$m_{i21} = -P_{A,i} a_i \sinh\, a_i x$$

$$m_{i22} = \cosh\, a_i x$$

$$m_{i31} = \frac{k_{1i}}{P_{Bi}(a_i^2 - b_i^2)}(\cosh\ b_i x - \cos\ a_i x)$$

$$m_{i32} = \frac{k_{1i}}{P_{Ai}P_{Bi}(a_i^2 - b_i^2)} \times \left[\frac{1}{a_i}\sinh\ a_i x - \frac{1}{b_i}\sinh\ b_i x\right]$$

$$m_{i33} = \cosh\ b_i x$$

$$m_{i34} = -\frac{\sinh\ b_i x}{P_{B,i}b_i}$$

$$m_{i41} = \frac{k_{1i}}{P_{A,i}(a_i^2 - b_i^2)}(a_i \sinh\ a_i x - b_i \sinh\ b_i x)$$

$$m_{i42} = \frac{k_{1i}}{P_{A,i}(a_i^2 - b_i^2)}(\cosh\ b_i x - \cosh\ a_i x)$$

$$m_{i43} = -P_{B,i}b_i \sinh\ b_i x$$

$$m_{i44} = \cosh\ b_i x$$

$$m_{i51} = \frac{k_{2i}}{P_{C,i}(a_i^2 - c_i^2)}(\cosh\ c_i x - \cosh\ a_i x)$$

$$m_{i52} = \frac{k_{2i}}{P_{A,i}P_{ci}(a_i^2 - c_i^2)} \times \left[\frac{1}{a_i}\sinh\ a_i x - \frac{1}{c_i}\sinh\ c_i x\right]$$

$$m_{i55} = \cosh\ c_i x$$

$$m_{i56} = -\frac{\sinh\ c_i x}{P_{C,i}c_i}$$

$$m_{i61} = \frac{k_{2i}}{(a_i^2 - c_i^2)}(a_i \sinh\ a_i x - c_i \sinh\ c_i x)$$

$$m_{i62} = \frac{k_{2i}}{P_{A,i}(a_i^2 - c_i^2)}(\cosh\ c_i x - \cosh\ a_i x)$$

$$m_{i65} = -P_{C,i}c_i \sinh\ c_i x$$

$$m_{i66} = \cos\ c_i x$$

$$m_{i71} = \frac{k_{3i}k_{1i}}{P_{D,i}P_{B,i}(a_i^2 - b_i^2)} \times \left[\frac{1}{b_i^2}(1 - \cosh\ b_i x) + \frac{1}{a_i^2}(\cosh\ a_i x - 1)\right] + \frac{k_{4i}k_{2i}}{P_{D,i}P_{C,i}(a_i^2 - c_i^2)} \times \left[\frac{1}{c_i^2}(1 - \cosh\ c_i x) + \frac{1}{a_i^2}(\cosh\ a_i x - 1)\right] + \frac{k_{5i}}{P_{D,i}a_i^2}(1 - \cosh\ 'a_i x)$$

$$m_{i72} = \frac{k_{3i}k_{1i}}{P_{D,i}P_{A,i}P_{B,i}(a_i^2 - b_i^2)} \times \left[\frac{1}{b_i^3}\sinh\ b_i x - \frac{1}{a_i^3}\sinh\ a_i x + \frac{x}{a_i^2} - \frac{x}{b_i^2}\right] + \frac{k_{4i}k_{2i}}{P_{D,i}P_{C,i}P_{A,i}(a_i^2 - c_i^2)} \times \left[\frac{1}{c_i^3}\sinh\ c_i x - \frac{1}{a_i^3}\sinh\ a_i x + \frac{x}{a_i^2} - \frac{x}{c_i^2}\right] + \frac{k_{5i}}{P_{D,i}P_{A,i}a_i^3}(\sinh\ a_i x - a_i x)$$

$$m_{i73} = \frac{k_{3i}}{P_{D,i}b_i^2}(1 - \cosh\ b_i x)$$

$$m_{i74} = \frac{\sinh\ b_i x - b_i x}{P_{D,i}b_i}$$

$$m_{i75} = \frac{k_{4i}}{P_{D,i}c_i^2}(1 - \cos\ c_i x)$$

$$m_{i76} = \frac{\sinh\ c_i c - c_i x}{P_{D,i}c_i}$$

$$m_{i77} = 1$$

$$m_{i78} = -\frac{x}{P_{D,i}}$$

$$m_{i81} = \frac{k_{3i}k_{1i}}{P_{B,i}(a_i^2 - b_i^2)}\left[\frac{1}{b_i}\sinh\ b_i x - \frac{1}{a_i}\sinh\ a_i x\right] + \frac{k_{4i}k_{2i}}{P_{C,i}(a_i^2 - c_i^2)} \times \left[\frac{1}{c_i}\sinh\ c_i x - \frac{1}{a_i}\sinh\ a_i x\right] + \frac{k_{5i}}{a_i}\sinh\ a_i x$$

$$m_{i82} = \frac{k_{3i}k_{1i}}{P_{A,i}P_{B,i}(a_i^2 - b_i^2)}$$

$$\times\left[\frac{1}{a_i^2}\cosh a_i x-\frac{1}{b_i^2}\cosh b_i x+\frac{1}{b_i^2}-\frac{1}{a_i^2}\right]$$

$$+\frac{k_{4i}k_{2i}}{P_{A,i}P_{C,i}\left(a_i^2-c_i^2\right)}$$

$$\times\left[\frac{1}{a_i^2}\cosh a_i x-\frac{1}{c_i^2}\cosh c_i x+\frac{1}{c_i^2}-\frac{1}{a_i^2}\right]$$

$$+\frac{k_{5i}}{P_{A,i}a_i^2}(1-\cosh a_i x)$$

$$m_{i83}=\frac{k_{3i}}{b_i}\sinh b_i x$$

$$m_{i84}=1-\cosh b_i x$$

$$m_{i85}=\frac{k_{4i}}{c_i}\sinh c_i x$$

$$m_{i86}=1-\cosh c_i x$$

$$m_{i87}=0$$

$$m_{i88}=1$$

For the full-thickness model the stratum corneum coefficient matrix is represented by the following:

$$\begin{bmatrix}1 & -h_i/P_{A,i} & 0 & 0 & 0 & 0 & 0 & 0\\ 0 & 1 & 0 & 0 & 0 & 0 & 0 & 0\\ 0 & 0 & 1 & 0 & 0 & 0 & 0 & 0\\ 0 & 0 & 0 & 1 & 0 & 0 & 0 & 0\\ 0 & 0 & 0 & 0 & 1 & 0 & 0 & 0\\ 0 & 0 & 0 & 0 & 0 & 1 & 0 & 0\\ 0 & 0 & 0 & 0 & 0 & 0 & 1 & 0\\ 0 & 0 & 0 & 0 & 0 & 0 & 0 & 1\end{bmatrix}$$

The previous general matrix (Eq. 22) when evaluated at the thickness of the i-th layer yields the following matrix equation:

$$\begin{bmatrix}U_{A,i}\\ F_{A,i}\\ U_{B,i}\\ F_{B,i}\\ U_{C,i}\\ F_{C,i}\\ U_{D,i}\\ F_{D,i}\end{bmatrix}=\boldsymbol{M}_i\cdot\begin{bmatrix}U_{A,i-1}\\ F_{A,i-1}\\ U_{B,i-1}\\ F_{B,i-1}\\ U_{C,i-1}\\ F_{C,i-1}\\ U_{D,i-1}\\ F_{D,i-1}\end{bmatrix}\qquad(23)$$

where $\boldsymbol{M}_i$ represents the matrix evaluated at the thickness, h_i. Applying this to each successive layer results in the following:

$$\begin{bmatrix}U_{A,n}\\ F_{A,n}\\ U_{B,n}\\ F_{B,n}\\ U_{C,n}\\ F_{C,n}\\ U_{D,n}\\ F_{D,n}\end{bmatrix}=[\boldsymbol{M}_n\boldsymbol{M}_{n-1}\boldsymbol{M}_2\boldsymbol{M}_1]\cdot\begin{bmatrix}U_{A,0}\\ F_{A,0}\\ U_{B,0}\\ F_{B,0}\\ U_{C,0}\\ F_{C,0}\\ U_{D,0}\\ F_{D,0}\end{bmatrix}\qquad(24)$$

where the coefficient matrix is the product of each of the matrices. This resulting matrix can be expressed as follows:

$$\begin{bmatrix}m_{11} & m_{12} & 0 & 0 & 0 & 0 & 0 & 0\\ m_{21} & m_{22} & 0 & 0 & 0 & 0 & 0 & 0\\ m_{31} & m_{32} & m_{33} & m_{34} & 0 & 0 & 0 & 0\\ m_{41} & m_{42} & m_{43} & m_{44} & 0 & 0 & 0 & 0\\ m_{51} & m_{52} & 0 & 0 & m_{55} & m_{56} & 0 & 0\\ m_{61} & m_{62} & 0 & 0 & m_{65} & m_{66} & 0 & 0\\ m_{71} & m_{72} & m_{73} & m_{74} & m_{75} & m_{76} & m_{77} & m_{78}\\ m_{81} & m_{82} & m_{83} & m_{84} & m_{85} & m_{86} & 0 & m_{88}\end{bmatrix}$$

All the development necessary to yield explicit concentration-distance expressions through the entire skin thickness for both the bilaminate and trilaminate models (each with full thickness and the tape stripped variants) has been accomplished.

Once the parameters for a particular MTX diester have been inserted (donor concentration, diffusivities, permeabilities, thickness) it is only necessary to algebraically solve for the 8×1 vector (to the right of the equals sign in Eq. 24). Depending on whether the model is trilaminate or bilaminate, stripped or full-thickness, certain parameters may not be necessary and others will be zero, either based on sink conditions or lack of back diffusion across the stratum corneum of α-monoester, γ-monoester, or MTX.

An example of such a situation can be shown with the full-thickness bilaminate model. Here the coefficient matrix (from Eq. 24) is evaluated

at its thickness which represents the thickness of the layer this matrix describes:

$$\begin{bmatrix} U_{A,2} \\ F_{A,2} \\ U_{B,2} \\ F_{B,2} \\ U_{C,2} \\ F_{C,2} \\ U_{D,2} \\ F_{D,2} \end{bmatrix} = \begin{bmatrix} m_{11} & m_{12} & 0 & 0 & 0 & 0 & 0 & 0 \\ m_{21} & m_{22} & 0 & 0 & 0 & 0 & 0 & 0 \\ m_{31} & m_{32} & m_{33} & m_{34} & 0 & 0 & 0 & 0 \\ m_{41} & m_{42} & m_{43} & m_{44} & 0 & 0 & 0 & 0 \\ m_{51} & m_{52} & 0 & 0 & m_{55} & m_{56} & 0 & 0 \\ m_{61} & m_{62} & 0 & 0 & m_{65} & m_{66} & 0 & 0 \\ m_{71} & m_{72} & m_{73} & m_{74} & m_{75} & m_{76} & m_{77} & m_{78} \\ m_{81} & m_{82} & m_{83} & m_{84} & m_{85} & m_{86} & 0 & m_{88} \end{bmatrix} \cdot \begin{bmatrix} U_{A,0} \\ F_{A,0} \\ U_{B,0} \\ F_{B,0} \\ U_{C,0} \\ F_{C,0} \\ U_{D,0} \\ F_{D,0} \end{bmatrix} \tag{25}$$

It follows that:

$$F_{A,0} = -m_{11}U_{A,0}/m_{12} \tag{26}$$

$$F_{A,2} = m_{21}U_{A,0} + m_{22}F_{A,0} \tag{27}$$

$$F_{B,2} = m_{41}U_{A,0} + m_{42}F_{A,0} \tag{28}$$

$$F_{C,2} = m_{61}U_{A,0} + m_{62}F_{A,0} \tag{29}$$

$$F_{D,2} = m_{81}U_{A,0} + m_{82}F_{A,0} \tag{30}$$

For the stratum corneum layer which lacks a metabolic component:

$$\begin{bmatrix} U_{A,1} \\ F_{A,1} \\ U_{B,1} \\ F_{B,1} \\ U_{C,1} \\ F_{C,1} \\ U_{D,1} \\ F_{D,1} \end{bmatrix} = \begin{bmatrix} 1 & -h_1/P_{A,1} & 0 & 0 & 0 & 0 & 0 & 0 \\ 0 & 1 & 0 & 0 & 0 & 0 & 0 & 0 \\ 0 & 0 & 1 & 0 & 0 & 0 & 0 & 0 \\ 0 & 0 & 0 & 1 & 0 & 0 & 0 & 0 \\ 0 & 0 & 0 & 0 & 1 & 0 & 0 & 0 \\ 0 & 0 & 0 & 0 & 0 & 1 & 0 & 0 \\ 0 & 0 & 0 & 0 & 0 & 0 & 1 & 0 \\ 0 & 0 & 0 & 0 & 0 & 0 & 0 & 1 \end{bmatrix} \cdot \begin{bmatrix} U_{A,0} \\ F_{A,0} \\ U_{B,0} \\ F_{B,0} \\ U_{C,0} \\ F_{C,0} \\ U_{D,0} \\ F_{D,0} \end{bmatrix} \tag{31}$$

It can then be obtained that:

$$U_{A,1} = U_{A,0} - h_1F_{A,0}/P_{A,1} \tag{32}$$

$$F_{A,1} = F_{A,0} \tag{33}$$

The cutaneous layer, which is composed of the viable epidermis and dermis, is also evaluated at its thickness:

$$\begin{bmatrix} U_{A,2} \\ F_{A,2} \\ U_{B,2} \\ F_{B,2} \\ U_{C,2} \\ F_{C,2} \\ U_{D,2} \\ F_{D,2} \end{bmatrix} = \begin{bmatrix} m_{211} & m_{212} & 0 & 0 & 0 & 0 & 0 & 0 \\ m_{221} & m_{222} & 0 & 0 & 0 & 0 & 0 & 0 \\ m_{231} & m_{232} & m_{233} & m_{234} & 0 & 0 & 0 & 0 \\ m_{241} & m_{242} & m_{243} & m_{244} & 0 & 0 & 0 & 0 \\ m_{251} & m_{252} & 0 & 0 & m_{255} & m_{256} & 0 & 0 \\ m_{261} & m_{262} & 0 & 0 & m_{265} & m_{266} & 0 & 0 \\ m_{271} & m_{272} & m_{273} & m_{274} & m_{275} & m_{276} & m_{277} & m_{278} \\ m_{281} & m_{282} & m_{283} & m_{284} & m_{285} & m_{286} & 0 & m_{288} \end{bmatrix} \cdot \begin{bmatrix} U_{A,1} \\ F_{A,1} \\ U_{B,1} \\ F_{B,1} \\ U_{C,2} \\ F_{C,2} \\ U_{D,2} \\ F_{D,2} \end{bmatrix} \tag{34}$$

It follows that:

$$U_{B,1} = -(m_{231}U_{A,1} + m_{232}F_{A,1})/m_{233} \tag{35}$$

$$U_{C,1} = -(m_{251}U_{A,1} + m_{252}F_{A,1})/m_{255} \tag{36}$$

$$U_{D,1} = -(m_{271}U_{A,1} + m_{272}F_{A,1} + m_{273}U_{B,1} + m_{275}U_{C,1})/m_{277} \tag{37}$$

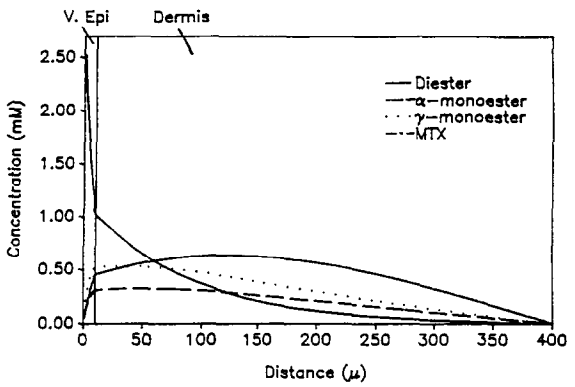

Fig. 3. Illustration of a concentration-distance profile in the tape-stripped skin for a theoretical set of parameters listed in Table 1 with different epidermal and dermal parameters.

Thus, all of the needed quantities have been determined and simulation of a resulting concentration distance profile is relatively simple. Similar determinations are performed for the bilaminate stripped, trilaminate stripped and trilaminate full-thickness models.

Briefly, the operative specific boundary conditions for each of the other three models are as follows: For the full-thickness trilaminate model, the same conditions are utilized as in the above example for the fluxes and concentrations at the donor and receptor planes. The only difference is that an intermediary viable epidermal layer exists and the algebra is slightly more complicated.

For the stripped models (bilaminate and trilaminate), the stratum corneum is absent, therefore, there is a finite flux for all four species not only at the receptor, but also at the donor plane. This accounts for the back diffusion of monoesters and MTX which has been actually observed in tape stripped experiments. Also, for mathematical simplicity, sink conditions are operative for monoesters and MTX at the donor plane. Obviously, since there is no stratum corneum, it is mathematically eliminated from this model, and its matrix is not utilized in the calculations.

Even though the preceding mathematical development is not extremely difficult conceptually, the mathematical operations, e.g., matrix multiplication, algebraic solution for unknown quantities, and the actual calculation of the concentration of each species at each distance x are next to impossible manually. With the aid of a microcomputer and the BASIC programming language, all

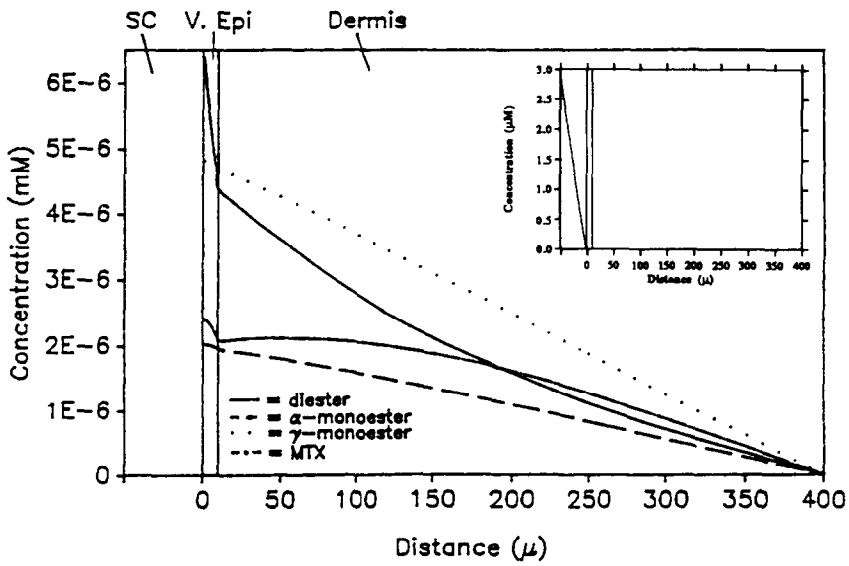

Fig. 4. Illustration of a concentration-distance profile in the full-thickness skin for a theoretical set of parameters listed in Table 1 with different epidermal and dermal parameters. Inset emphasizes stratum corneum concentration gradient.

Table 1
Parameters for demonstration of stripped and full-thickness skin concentration-distance profiles

Parameter	Fig. 3	Fig. 4
P_{sc} (cm/h)	–	6.0×10^{-4}
P_AEpi (cm^2/h)	6.0×10^{-4}	0.6
P_BEpi (cm^2/h)	6.0×10^{-4}	0.6
P_CEpi (cm^2/h)	6.0×10^{-4}	0.6
P_DEpi (cm^2/h)	6.0×10^{-4}	0.6
k_1Epi (1/h)	200	20000
k_2Epi (1/h)	400	40000
k_3Epi (1/h)	100	1000
k_4Epi (1/h)	200	20000
k_5Epi (1/h)	50	50000
P_ADerm (cm^2/h)	5.0×10^{-3}	5
P_BDerm (cm^2/h)	5.0×10^{-3}	5
P_CDerm (cm^2/h)	5.0×10^{-3}	5
P_DDerm (cm^2/h)	5.0×10^{-3}	5
k_1Derm (1/h)	20	2000
k_2Derm (1/h)	40	4000
k_3Derm (1/h)	10	1000
k_4Derm (1/h)	20	2000
k_5Derm (1/h)	5	5000

Epidermis thickness, 0.001 cm; dermis thickness, 0.04 cm; donor concentration, 2×10^{-3} M; stratum corneum thickness, 0.005 cm.

that is required is the insertion of the parameters for a prodrug into one of four computer programs which simulate trilaminate stripped, trilaminate full-thickness, bilaminate stripped, and bilaminate full-thickness models, and the entire concentration-distance profile for a prodrug is generated.

2. Discussion

An illustration of profiles resulting from hypothetical sets of parameters inserted into the trilaminate model (full-thickness and stripped) have been presented in Fig. 3 and 4. In Fig. 3, simulations from the trilaminate stripped models have been illustrated which employed different epidermal and dermal parameters. The full-thickness counterpart of this is shown in Fig. 4. All of the parameters utilized in the generation of these two figures are presented in Table 1.

At this stage of development these models are only intended to be used for illustrative purposes. They serve as useful means of delineating certain critical parameters of a drug molecule that can affect its concentration-distance profile. An example of this type of illustration will be shown with a series of compounds like the MTX dialkyl esters for which some experimental parameters are available (Fort and Mitra, 1989).

For the MTX dialkyl ester series, the experimentally determined parameters such as the full-thickness and stripped permeabilities (Fort et al., 1993, 1994), have been utilized with other arbitrary but reasonable parameters. Dipropyl MTX and diisopropyl MTX are given identical permeabilities in the dermis and epidermis. Dibutyl MTX is given an epidermal permeability based on the linear decline of this parameter from dimethyl MTX, to diisopropyl MTX. With these compounds it is not explicitly known what the enzymatic rate constants for bioconversion are within the skin layers. However, the relative rate constants for this series of compounds have been determined in homogenates (Fort and Mitra, 1989). Dermis diffusivities are obtained from the literature for similar compounds (Yu et al., 1980c), on which there does not seem to be a great structural dependence. Moreover, an adjustment has been made for molecular weight, e.g., the diffusivity is decreased proportionally to the cube root of the molecular weight. According to the experiments conducted in this project where the dermal and epidermal hydrolysis rates are compared, the dermis is found to have ester hydrolase activity roughly 10-times that of the epidermis in the same area of the skin. However, when a slightly less complicated model utilized by Yu et al. (1980a) was iterated with extensive experimental data it was shown that the viable epidermis had a more significant esterase metabolic component than the dermis in the intact skin. It is also obvious from the data in the present work that when considering the stripped skin studies, the donor flux of monoesters averages 5–10-times that of the receptor monoester fluxes. This can only occur if the concentration gradient is skewed toward the donor side of the membrane. Such a gradient would be present for two reasons: (1) if the epidermal permeability was lower than the dermis, which it is; and (2) if the epidermal rate

constants are greater than that for the dermis. From extensive experimentation with the models by varying the parameters, it has been shown that to consistently produce higher theoretical donor monoester fluxes over the receptor, both conditions are necessary. Therefore, for the sake of this illustrative procedure, the epidermal rate constants are considered exactly 10-times those of the dermis.

The actual parameters used in this stripped skin illustration are listed in Table 2. The hypothetically stripped skin profiles for MTX and dipropyl MTX are shown in Fig. 5 and 6, while the full-thickness skin profiles are shown in Fig. 7 and 8. Full-thickness skin parameters are also listed in Table 2. To compare the profiles from equimolar applied concentrations of compounds having different parameters, the same donor concentration of each compound has been utilized in the simulations.

With a compound like MTX that is not metabolized as it crosses the stripped skin, the gradient in the membrane is perfectly linear. With the diesters, as the metabolic component increases, the gradient becomes slightly non-linear. The effects of differences in diffusivity between the epidermis and dermis on the concentration gradient are apparent. It is very steep in the epidermis and less so in the dermis. This is true irrespective of whether or not the parent drug is further metabolized.

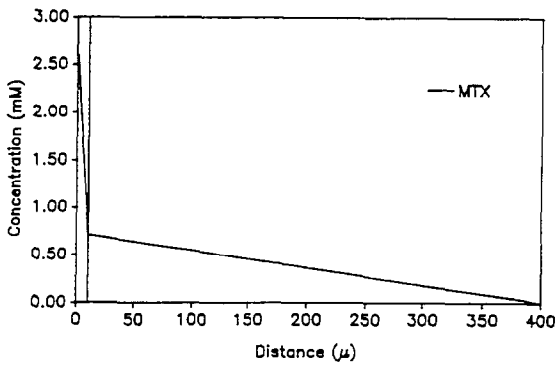

Fig. 5. Illustration of a concentration-distance profile in the tape-stripped skin for a reasonable set of parameters assigned to MTX (from Table 2).

In using the same parameters from the stripped skin simulations, it can be shown that the most important factor in attaining high concentrations

Table 2
Parameters for stripped skin and full-thickness skin concentraton-distance profiles

Parameter	Stripped skin		Full-thickness skin	
	MTX	DPMTX	MTX	DPMTX
P_{sc}	–	–	5.644×10^{-5}	1.162×10^{-4}
P_AEpi (cm^2/h)	3.978×10^{-5}	2.494×10^{-5}	3.978×10^{-5}	2.494×10^{-5}
P_BEpi (cm^2/h)	–	3.862×10^{-5}	–	3.862×10^{-5}
P_CEpi (cm^2/h)	–	3.862×10^{-5}	–	3.862×10^{-5}
P_DEpi (cm^2/h)	–	3.978×10^{-5}	–	3.978×10^{-5}
k_1Epi (1/h)	–	12.295	–	12.295
k_2Epi (1/h)	–	21.555	–	21.555
k_3Epi (1/h)	–	1×10^{-5}	–	1×10^{-5}
k_4Epi (1/h)	–	1×10^{-5}	–	1×10^{-5}
k_5Epi (1/h)	–	1×10^{-6}	–	1×10^{-6}
P_ADerm (cm^2/h)	4.6×10^{-3}	4.35×10^{-3}	4.6×10^{-3}	4.35×10^{-3}
P_BDerm (cm^2/h)	–	4.47×10^{-3}	–	4.47×10^{-3}
P_CDerm (cm^2/h)	–	4.47×10^{-3}	–	4.47×10^{-3}
P_DDerm (cm^2/h)	–	4.6×10^{-3}	–	4.6×10^{-3}
k_1Derm (1/h)	–	1.230	–	1.230
k_2Derm (1/h)	–	2.156	–	2.156
k_3Derm (1/h)	–	1×10^{-5}	–	1×10^{-5}
k_4Derm (1/h)	–	1×10^{-5}	–	1×10^{-5}
k_5Derm (1/h)	–	1×10^{-6}	–	1×10^{-6}

Epidermis thickness, 0.001 cm; dermis thickness, 0.04 cm; donor concentration, 2×10^{-3} M; for full-thickness skin, the stratum corneum thickness = 0.005 cm.

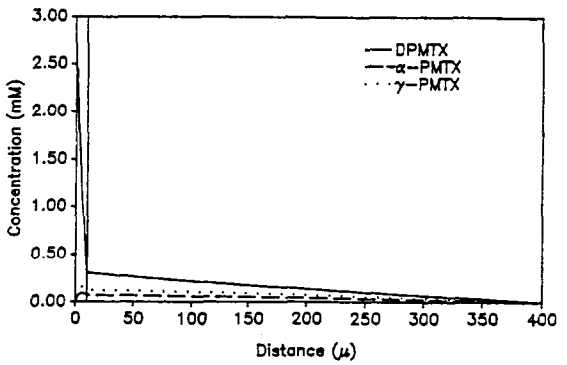

Fig. 6. Illustration of a concentration-distance profile in the tape-stripped skin for a reasonable set of parameters assigned to DPMTX (from Table 2).

at the level of the viable epidermis is the stratum corneum permeability. The relative concentrations achieved at the epidermal site are roughly in proportion to the stratum corneum permeability values. Another important observation is that the concentrations generated at the level of the viable epidermis in both the full-thickness and stripped skin simulations are proportional to the differences in permeabilities of the compounds between these layers, e.g., 100–1000-fold differences. In the full-thickness case a large reduction in concentration occurs due to the very steep

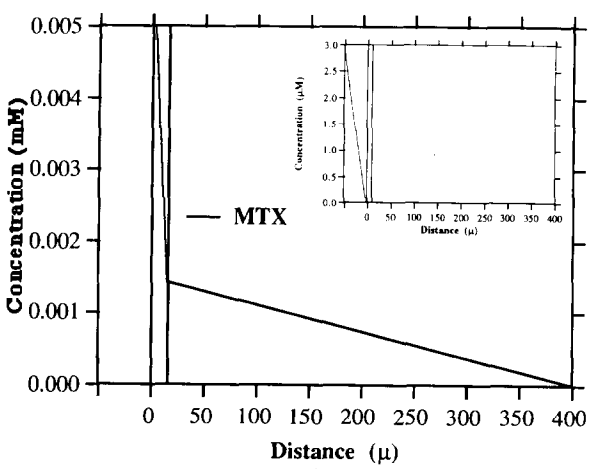

Fig. 7. Illustration of a concentration-distance profile in the full-thickness skin for a reasonable set of parameters assigned to MTX (from Table 2). Inset emphasizes stratum corneum concentration.

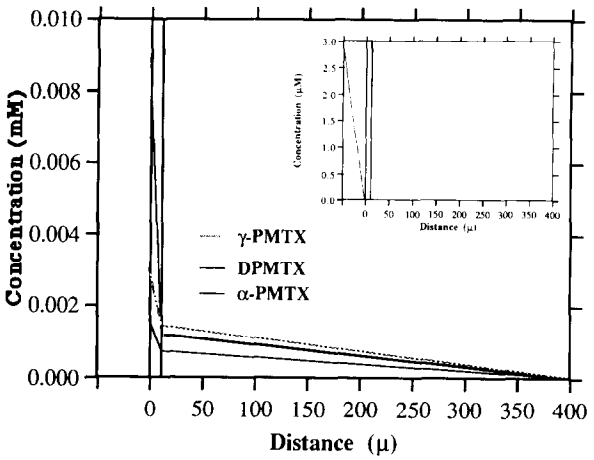

Fig. 8. Illustration of a concentration-distance profile in the full-thickness skin for a reasonable set of parameters assigned to DPMTX (from Table 2). Inset emphasizes stratum corneum concentration gradient.

gradient across the stratum corneum which is shown in the insets of Fig. 7 and 8. The concentration on the donor side of the stratum corneum would be 2×10^{-3} M.

The highest concentration observed in the viable epidermis is with dimethyl MTX which is still at best 1/70 of the donor concentration. It is important to realize, though, that the concentrations are expressed in terms of the donor and receptor solutions. Since the exact partition coefficient between the epidermis and the donor solution is not known for any of the compounds, the illustrated concentrations do not take partitioning into account. More lipophilic compounds would be expected to yield higher concentration in the epidermis due to partitioning, although dermal partition coefficients are close to unity (Yu et al., 1979b).

The main purpose of this exercise is to illustrate, in general, the variation in profiles for a series of diester homologues. From these profiles, suggestions as to future molecular modifications, or other system changes can be obtained. If the goal is to yield the parent compound in the viable epidermis, the suggestion would be to design a compound which would be cleaved all the way to MTX. It is shown with the present homologues, that those cleaved the most rapidly to the inter-

mediate monoesters, yield the highest monoester concentration at the level of epidermis, Complete regeneration of the parent compound at a high rate would be extremely advantageous. Since the most permeable compound, dimethyl MTX, yields the highest concentration at the level of the viable epidermis, any molecular modification that would be necessary to yield good bioconversion tendencies should not compromise on the stratum corneum permeability of the compound. It may be possible to synthesize a compound yielding high ester hydrolysis rates as shown with dipropyl MTX and dibutyl MTX, and utilize penetration enhancers to increase their permeability, since it shows that the more lipophilic compounds in this series (higher than dimethyl MTX) had lower permeability.

Although in this discussion, the comparison between compounds is largely illustrative, it may be possible in the future to concentrate on one or two of the presently studied compounds or possibly a new derivative and perform more extensive simulations. Such simulations would be to further sub-divide the skin into individual layers to assess exact dermis and epidermis permeabilities, perhaps in the presence of enzyme inhibitors. Also, different concentrations of compounds could be used to ascertain the degree to which the system enzymes have become saturated, leading to subsequent K_m and V_{max} determination. Model extensions could then be developed which take these factors into consideration, with the ultimate goal of comparing more accurately generated concentration-distance profiles with a profile of efficacy of a compound applied topically to an animal or human by a zero-order device. Such an endeavor can hopefully yield the most sought after endpoint in rational drug design, a safe and effective topical drug, in this case an effective antipsoriatic agent.

In conclusion, our proposed models provide a predictive tool and can be used as a basis for developing a research strategy for the discovery and development of compounds with superior skin permeation characteristics. The drawbacks of this approach lies in the fact that several parameters need to be determined experimentally prior to any actual simulations. Such parameters include the thickness of each diffusion barrier, permeability coefficients of a prodrug and its metabolites, and individual bioreversion rate constant in each layer. In addition, the reliability of a predicted concentration-time profile can only be confirmed through microtoming a frozen tissue sample and analyzing the concentrations of individual product in each skin section.

Glossary

Symbol	Meaning
$k_{n,i}$	first order metabolic rate constants in the ith layer
Subscript A–D	diester, α-monoester, γ-monoester, MTX
a_i, b_i, c_i	hybrid constants obtained from $k_{n,i}$ and D as shown in Eq. 5–7
D	diffusion coefficient in a certain layer
K	partition coefficient
P	permeability coefficient
F	flux
$\boldsymbol{M}_i$	matrix evaluated at thickness h_i

Acknowledgments

This work was supported in part by a grant from American Cyanamid Co., Pearl River, NY, and in part by NIH grant NS 25284.

References

Ando, H.Y., Ho, N.F.H. and Higuchi, W.I., In vitro estimates of topical bioavailability. *J. Pharm. Sci.*, 66 (1977a) 755–757.

Ando, H.Y., Ho, N.F.H. and Higuchi, W.I., Skin as an active metabolizing barrier: I. Theoretical analysis of topical bioavailability. *J. Pharm. Sci.*, 66 (1977b) 1525–1528.

Bissett, D.L., Anatomy and biochemistry of skin. In Kydoneius, A.F. and Berner, B. (Eds), *Transdermal Delivery of Drugs*, Vol. 1, CRC Press, Boca Raton, FL, 1987, pp. 29–42.

Fort, J.J. and Mitra, A.K., Permeability and bioconversion characteristics of methotrexate mono- and dialkyl esters in hairless mouse skin. *Int. J. Pharm.*, 102 (1994) 241–247.

Fort, J.J., Shao, Z. and Mitra, A.K., Transport and degradation characteristics of methotrexate dialkyl ester prodrugs across tape-stripped hairless mouse skin. *Int. J. Pharm.*, 100 (1993) 233–239.

Fort. J.J., Shao, Z. and Mitra, A.K., Transport of methotrexate dialkyl ester prodrugs across full-thickness mouse skin. *Drug. Dev. Ind. Pharm.*, (1994) In press.

Fox, J.L., Yu, C.D., Higuchi, W.I. and Ho, N.F.H., General Physical model for simultaneous diffusion and metabolism in biological membranes. The computational approach for the steady-state case. *Int. J. Pharm.*, 2 (1979) 41–57.

Higuchi, W.I., Gordon, N.A., Fox, J.L. and Ho, N.F.H., Transdermal delivery of prodrugs. *Drug Dev. Ind. Pharm.*, 9 (1983) 691–706.

Loftsson, T., Experimental and theoretical model for studing simultaneous transport and metabolism of drugs in excised skin. *Arch. Pharm. Chem. Sci. Ed.*, 10 (1982) 17–24.

Wallace, S.M. and Barnett, G., Pharmacokinetic analysis of percutaneous absorption: evidence of parallel penetration pathways for methotrexate. *J. Pharm. Biopharm.*, 6 (1978) 315–325.

Yu, C.D., Fox, J.L., Ho, N.F.H. and Higuchi, W.I., Physical model evaluation of topical prodrug delivery-simultaneous transport and bioconversion of vidarabine-5′-valerate: I. Physical model development. *J. Pharm. Sci.*, 68 (1979a) 1341–1346.

Yu, C.D., Fox, J.L., Ho, N.F.H. and Higuchi, W.I., Physical model evaluation of topical prodrug delivery-simultaneous transport and bioconversion of vidarabine-5′-valerate: II. Parameter determination. *J. Pharm. Sci.*, 68 (1979b) 1347–1357.

Yu, C.D., Gordon, N.A., Fox, J.L., Higuchi, W.I. and Ho, N.F.H., Physical model evaluation of topical prodrug delivery-simultaneous transport and bioconversion of vidarabine-5′-valerate: V. Mechanistic analysis of influence of nonhomogeneous enzyme distributions in hairless mouse skin. *J. Pharm. Sci.*, 69 (1980a) 775–780.

Yu, C.D., Fox, J.L., Higuchi, W.I. and Ho, N.F.H., Physical model evaluation of topical prodrug delivery-simultaneous transport and bioconversion of vidarabine-5′-valerate: IV. Distribution of esterase and deaminase enzymes in hairless mouse skin. *J. Pharm. Sci.*, 69 (1980b) 772–775.

Yu, C.D., Higuchi, W.I., Ho, N.F.H., Fox, J.L. and Flynn, G.L., Physical model evaluation of topical prodrug delivery-simultaneous transport and bioconversion of vidarabine-5′-valerate: III. Permeability differences of vidarabine and n-pentanol in components of hairless mouse skin. *J. Pharm. Sci.*, 69 (1980c) 770–772.